Journal of Aerosol Science 54 (2012) 32–48

Contents lists available at SciVerse ScienceDirect

Journal of Aerosol Science

journal homepage: www.elsevier.com/locate/jaerosci

A TEMOM model to simulate nanoparticle growth in the temporal mixing layer due to Brownian coagulation

Ming-Liang Xie [a,b,*], Ming-Zhou Yu [c], Lian-Ping Wang [b]

[a] The State Key Laboratory of Coal Combustion, Huazhong University of Science and Technology, Wuhan 430074, PR China
[b] Departmental of Mechanical Engineering, University of Delaware, Newark, DE 19716, USA
[c] China Jiliang University, Hangzhou 310018, PR China

ARTICLE INFO

Article history:
Received 5 April 2012
Received in revised form
5 July 2012
Accepted 5 July 2012
Available online 25 July 2012

Keywords:
Nanoparticles
Coagulation
Taylor-series expansion method of moment
Direct numerical simulation
Temporal mixing layer

ABSTRACT

In the present study, a compact and fast MATLAB program coupled with the Taylor-series expansion method of moments (TEMOM) was developed to simulate the effect of coherent structures on the particle Brownian coagulation in the temporal mixing layer. The distributions of number concentration, mass concentration and particle average volume driven by coagulation, advection and diffusion are obtained. The developed TEMOM method has no prior requirement for the particle size distribution (PSD), and it is a promising method to approximate the aerosol general dynamics equation (GDE). The fluid and particle fields are coupled together and are presented with three non-dimensional parameters (i.e., Reynolds number, *Re*; Schmidt number based on particle moment, Sc_M, and Damkohler number, *Da*) in the governing equations. The temporal evolutions of the first three moments are discussed for different Damkohler numbers ($Da=0.5$, 1.0, 2.0). As the fluid flow evolves in time, the number concentration of nanoparticles decreases gradually, while the particle average volume increase. The distribution of number concentration, mass concentration, and average volume of nanoparticles are spatially inhomogeneous due to the mixing of coherent vortex structures. Far away from the eddy structure, the effect of the fluid advection on particle coagulation is small; however, the particle coagulation within the eddy core has an obvious wave-like distribution because of the large-scale eddy. The results reveal that the coherent structures play a significant role in the particle Brownian coagulation in the mixing layer. The particle coagulation affects quantitatively the distribution of particle number concentration, volume concentration and average diameter, but the qualitative characteristics of these distributions remain unchanged.

1. Introduction

Aerosol particles are increasingly recognized as one of the most common unhealthy components of air pollution (Davidson et al., 2005). Particle size and concentration affect not only the environment but also the health of human beings. Researchers have already shown that there is a strong correlation between mortality and particle size, with specific reference from nano-particles (<50 nm) to fine particles (<2.5 mm) (Kittelson, 1998; Stone & Donaldson, 1998; Jacobson et al., 2005).

* Corresponding author.
E-mail address: mlxie@mail.hust.edu.cn (M.-L. Xie).

0021-8502/$ - see front matter © 2012 Elsevier Ltd. All rights reserved.
http://dx.doi.org/10.1016/j.jaerosci.2012.07.004

Nomenclature

A_1	the amplitude of the fundamental disturbances
A_2	the amplitude of the sub-harmonic disturbances
Da	the Damkohler number
D_n	the diffusion coefficient
K_b	the Boltzmann's constant
L	the characteristic length ($=\theta$)
M_k	the kth order moment of particle size distribution
M_{k0}	the initial value of kth order particle size distribution moment
M_0	the 0th moment that is the total particle number concentration
M_{00}	the initial value of 0th order particle size distribution moment
M_1	the 1st moment that is proportional to the total particle mass
M_{10}	the initial value of 1st order particle size distribution moment
M_2	the 2nd moment that is proportional to the total light scattered
M_{10}	the initial value of 2nd order particle size distribution moment
M_c	the dimensionless moment
M_{c0}	the initial value of dimensionless moment
N	the parameter for the log-normal distribution
Re	the Reynolds number
Sc_M	the Schmidt number based on the particle moment
T	the fluid temperature
U	the velocity difference across the mixing layer
U_1	the velocity of upper stream in the mixing layer
U_2	the velocity of upper stream in the mixing layer
V	the mean particle volume
V_0	the initial value of mean particle volume
c	the mean thermal speed
k	the order of Taylor series expansion
n	the number density of particles
t	the time variant
u	the velocity component in the coordinate x direction.
v	the velocity component in the coordinate y direction.
x	the horizontal coordinate
y	the vertical coordinate
α	the wave number of disturbances
α_p	the accommodation coefficient
β	the collision frequency function
ϕ_1	the eigenfunction of fundamental disturbances
ϕ_2	the eigenfunction of sub-harmonic disturbances
ψ	the stream function of disturbances
ρ	the fluid density
ρ_p	the particle density
ν	the kinetic viscosity
θ	the initial vorticity thickness of mixing layer
υ	the particle volume
υ_g	the geometric mean volume
κ	the size-independent diffusivity
σ	the standard deviation

The evolution of nano-particles is controlled by the general dynamic equation (GDE), which is a nonlinear partial differential equation (Friedlander, 2000). The GDE is capable of describing the particle evolution under all kinds of processes (i.e., advection, diffusion, coagulation, nucleation, surface growth and other physical or chemical phenomena, etc.). However, it is computationally demanding to directly solve the GDE mainly because of its dependence on the particle volume. As efficient alternatives, several scientific methods have been developed to address this shortcoming. Among these methods, the sectional method and nodal method (Prakash et al., 2003; Miller & Garrick, 2004; Garrick et al., 2006; Wang et al., 2007) divide the particle volume space into several discrete sections or bins. At each section or bin, the particle volume is considered as a constant or linearly distributed and the GDE can be solved. An even more efficient technique is the method of moment (MOM) (Pratsinis, 1988; Pratsinis & Kim, 1989; Settumba & Garrick, 2003; Chan et al., 2006; Lin et al., 2003; Lin and Liu, 2010). It considers the moments of the particle size distribution over the entire particle volume space. The GDE can be transformed into a set of independent moment equations. A closure problem arises when solving a finite number of moments, which requires the modeling of unsolved higher order moments in terms of solved lower order moments. These models can yield a close set of equations governing the solved lower order moments. The classical moment method usually addresses the closure problem by assuming that the particle size distribution is mono-dispersed or log-normally distributed. McGraw (1997) proposed a new method known as the quadrature method of moment (QMOM) to make the moment equations closed. Based on the theory of McGraw (1997), Fox (2003) further developed a new method named the direct quadrature method of moment (DQMOM), which has proved to be compatible with QMOM in case of mono-variant functions. DQMOM also offers a powerful numerical approach for describing the poly-disperse solids, which have undergone the segregation, growth, aggregation and breakage processes in the context of computational fluid dynamics (CFD) simulations. So far as the closure problem is concerned, the QMOM and DQMOM are more suitable for engineering applications because of not only the accuracy but also more importantly the higher computational efficiency. For the QMOM, the major problem is that it needs to additionally solve an eigenvalues and eigenvector problem. For the DQMOM, it amounts to solving a set of linear algebraic equations, and is more stable than the QMOM. Yu et al. (2008a) have recently presented a new numerical approach termed as the Taylor-series expansion method of moment

(TEMOM) to solve the coagulation equation. In the TEMOM, the closure of the moment equations is approached using the Taylor-series expansion technique. Through constructing a system of the three first-order ordinary differential equations, the most important moments for describing the aerosol dynamics, including the particle number density, particle mass and geometric standard deviation, are obtained. This approach has no prior requirement for the particle size spectrum, and the limitation inherent in the lognormal distribution theory automatically disappears.

In the present study, the nanoparticle-laden flow in the temporal mixing layer was investigated. There are two scientific problems to be solved, namely, the flow structure and particle evolution. Since the particles considered are very small (around nanometer in size), which means the Stokes number of particles St«1, the particles are assumed to follow the gas flow precisely. As a first step it is reasonable to consider the flow and the particle fields separately and neglect the effect of particles on the gas flow (Xie et al., 2007, 2009a, 2009b). The aim of this paper is to simulate the two-dimensional flow structures and particle evolution in the mixing layer. An compact and efficient direct numerical simulation scheme coupled with the Taylor-series expansion method of moments (TEMOM) will be developed to simulate the effect of coherent structures on the particle coagulation and growth in the flow field.

2. Mathematical modeling

2.1. Flow fields

The flow is considered to be the constant density two-dimensional temporal mixing layer containing the nano-scale particles. This temporal mixing layer can be thought of as an approximation to spatially developing mixing layer (Rogers & Moser, 1992; Moser & Rogers, 1993) and the simulation of time-developing mixing layer allows a much higher resolution for computation. For the temporal mixing layer, we can impose periodic boundary conditions in the stream-wise (x) direction. Considering that all the perturbations vanish rapidly as $y\to\infty$, where y is the coordinate in the transverse direction, periodic conditions can be also imposed in the transverse direction by introducing the image flows far enough from the mixing layer center. Thus, the standard Fourier pseudo-spectral method can be applied directly. A schematic of the temporal mixing layer is shown in Fig. 1. The primary transport variables for the flow field are the fluid velocity and pressure. These variables are governed by the Navier–Stokes equations:

$$\begin{aligned}
&\frac{\partial u}{\partial x}+\frac{\partial v}{\partial y}=0\\
&\frac{\partial u}{\partial t}+u\frac{\partial u}{\partial x}+v\frac{\partial u}{\partial y}=-\frac{1}{\rho}\frac{\partial p}{\partial x}+\nu\left(\frac{\partial^2 u}{\partial x^2}+\frac{\partial^2 u}{\partial y^2}\right)\\
&\frac{\partial v}{\partial t}+u\frac{\partial v}{\partial x}+v\frac{\partial v}{\partial y}=-\frac{1}{\rho}\frac{\partial p}{\partial y}+\nu\left(\frac{\partial^2 v}{\partial x^2}+\frac{\partial^2 v}{\partial y^2}\right)
\end{aligned}\tag{1}$$

where ρ is the fluid density; p is the pressure; ν is the kinematic viscosity; u, v are the velocity component in the x and y directions, respectively. The initial velocity for the time-developing mixing layer consists of the following two parts: the

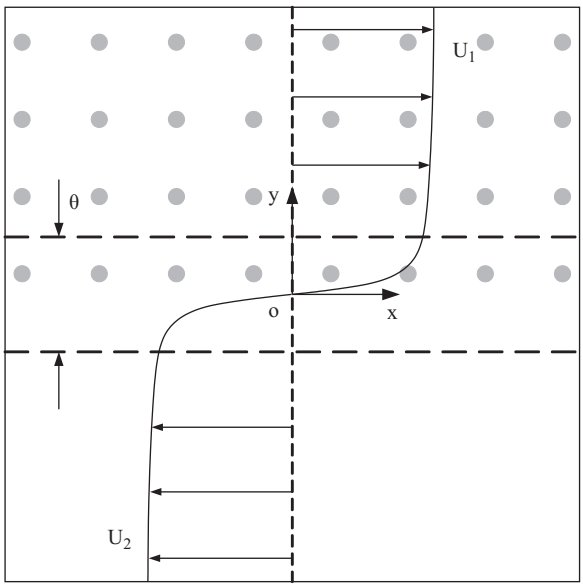

Fig. 1. The initial configuration of temporal mixing layer.

base flow and the corresponding disturbances. The transverse velocity v of base flow is set to zero and the streamwise velocity u is specified using a hyperbolic tangent profile:

$$u(x,y,0)=\frac{U_1+U_2}{2}+\frac{U_1-U_2}{2}\tan\left(\frac{y}{2\theta}\right) \tag{2}$$

where U_1 and U_2 $(=-U_1)$ are the far field velocities of two parallel streams on each side of the shear layer, and θ is the initial momentum thickness, and the upper and lower boundaries are slip walls. Using slip walls allows us to concentrate on the shear region without having to resolve the boundary layer on the lower and upper walls.

2.2. Particle fields

The transport of the nano-scale particles dispersed through the fluid is governed by the aerosol general dynamics equations (GDE). The GDE describes the particle dynamics under the effect of different physical and chemical processes: advection, diffusion, coagulation, surface growth, nucleation and the other internal/external forces (Friedlander, 2000). In the present study, only the Brownian coagulation in the free molecule regime is considered, and the GDE can be written as:

$$\frac{\partial n}{\partial t}+u\frac{\partial n}{\partial x}+v\frac{\partial n}{\partial y}=\frac{\partial}{\partial x}\left(D_n\frac{\partial n}{\partial x}\right)+\frac{\partial}{\partial y}\left(D_n\frac{\partial n}{\partial y}\right)+\left[\frac{dn}{dt}\right]_{coag} \tag{3}$$

the source term, $[dn/dt]_{coag}$ is given by

$$\left[\frac{dn}{dt}\right]_{coag}=\frac{1}{2}\int_0^v\beta(v_1,v-v_1)n(v_1,t)n(v-v_1,t)dv_1-\int_0^v\beta(v_1,v)n(v,t)n(v_1,t)dv_1 \tag{4}$$

which represents the effects of particle-particle interactions resulting in coagulation, and $n(v,t)dv$ is the number of particles with volume from v to $v+dv$ at time t; β is the collision frequency function for coagulation in free molecule regime, which is given by:

$$\beta=\left(\frac{3}{4\pi}\right)^{1/6}\left(\frac{6K_bT}{\rho_p}\right)^{1/2}\left(\frac{1}{v}+\frac{1}{v_1}\right)^{1/2}(v^{1/3}+{v_1}^{1/3})^2 \tag{5}$$

where K_b is the Boltzmann's constant; ρ_p is the particle density; and D_n is the diffusion coefficient in the free molecule regime, which is given by:

$$D_n=\frac{(3/4\pi)^{1/3}K_bT}{v^{2/3}\rho_p c(1+\pi\alpha_p/8)} \tag{6}$$

where c is the mean thermal speed; α_p is the accommodation coefficient; T is the fluid temperature, and the fluid in this study is the air at room temperature. From a practical point of view (Garrick et al., 2006; Settumba & Garrick, 2003), it is computationally unfeasible to directly solve the GDE except for the small range of discrete particle sizes. In order to overcome this problem, a moment method is utilized to describe the particle field in time and space. The kth order moment M_k of the particle distribution is defined as:

$$M_k=\int_0^v v^k n(v)dv \tag{7}$$

By multiplying both sides of the GDE with v^k and integrating over all particle sizes, a system of transport equations for M_k are obtained (Pratsinis, 1988). The transport equations for the kth order moment M_k is expressed as:

$$\frac{\partial M_k}{\partial t}+u\frac{\partial M_k}{\partial x}+v\frac{\partial M_k}{\partial y}=\frac{\partial}{\partial x}\left(\kappa\frac{\partial M_{k-2/3}}{\partial x}\right)+\frac{\partial}{\partial y}\left(\kappa\frac{\partial M_{k-2/3}}{\partial y}\right)+\left[\frac{dM_k}{dt}\right]_{coag} \tag{8}$$

where the size-independent diffusivity is $\kappa=D_n\times v^{2/3}$; $[dM_k/dt]_{coag}$ is the source term due to the Brownian coagulation and can be expressed as (Upadhyay & Ezekoye, 2003):

$$\left[\frac{dM_k}{dt}\right]_{coag}=\frac{1}{2}\int_0^\infty\int_0^\infty[(v+v_1)^k-v^k-{v_1}^k]\beta(v,v_1)n(v,t)n(v_1,t)dvdv_1,(k=0,1,2,\ldots) \tag{9}$$

The minimum number of moments required to close the moment equations is the first three, M_0, M_1 and M_2. The 0th moment M_0 is the total particle number concentration; the first moment M_1 is the total volume fraction and is proportional to the total particle mass concentration; the second moment M_2 is proportional to the total light scattered (Friedlander, 2000). According to the prior developed Taylor-series expansion method of moment (TEMOM) (Yu et al., 2008a, b, c), the source term in the first three moments can be written as:

$$\left[\frac{dM_0}{dt}\right]_{coag}=\frac{\sqrt{2}B_1(65{M_C}^2-1210M_C-9223){M_0}^2}{5184(M_0/M_1)^{1/6}}\quad\left[\frac{dM_1}{dt}\right]_{coag}=0\quad\left[\frac{dM_2}{dt}\right]_{coag}=-\frac{\sqrt{2}B_1(701{M_C}^2-4210M_C-6859){M_1}^2}{2592(M_0/M_1)^{1/6}} \tag{10}$$

where the constant $B_1=(3/4\pi)^{1/6}(6K_bT/\rho_p)^{1/2}$, and the three fractional moments $M_{-2/3}$, $M_{1/3}$ and $M_{4/3}$ appeared in the first three moment equations can be expressed as:

$$M_{-2/3}=\frac{(4+5M_C)M_0V^{-2/3}}{9};\ \ M_{1/3}=\frac{(10-M_C)M_0V^{1/3}}{9};$$
$$M_{4/3}=\frac{(7+2M_C)M_0V^{4/3}}{9} \tag{11}$$

in which $V=M_1/M_0$ is the mean particle size, and the dimensionless moment M_C is defined as:

$$M_C=\frac{M_2M_0}{{M_1}^2} \tag{12}$$

2.3. Non-dimensionalization

The governing equations are non-dimensionalized to simplify the treatment and analysis of the interactions between the hydrodynamic and particle fields. It can be accomplished using the following relations:

$$t^*=\frac{t}{L/U};\ \ x^*=\frac{x}{L};\ \ y^*=\frac{y}{L};\ \ u^*=\frac{u}{U};\ \ v=\frac{v}{U};\ \ p^*=\frac{p}{\rho U^2};$$
$${M_k}^*=\frac{M_k}{M_{k0}};\ \ V^*=\frac{V}{V_0};\ \ {M_C}^*=\frac{M_C}{M_{C0}} \tag{13}$$

in which the characteristic length L is the initial momentum thickness of the mixing layer (θ); the characteristic velocity U is the velocity difference across the mixing layer ($2U_1$); M_{k0} is the initial value of the kth moment. Substituting the relations given in Eq. (13) into Eq. (1) yields the familiar mass and momentum conservation equations (for brevity, the star symbol '$*$' is omitted thereafter):

$$\frac{\partial u}{\partial x}+\frac{\partial v}{\partial y}=0$$
$$\frac{\partial u}{\partial t}+u\frac{\partial u}{\partial x}+v\frac{\partial u}{\partial y}=-\frac{\partial p}{\partial x}+\frac{1}{Re}\left(\frac{\partial^2 u}{\partial x^2}+\frac{\partial^2 u}{\partial y^2}\right)$$
$$\frac{\partial v}{\partial t}+u\frac{\partial v}{\partial x}+v\frac{\partial v}{\partial y}=-\frac{\partial p}{\partial y}+\frac{1}{Re}\left(\frac{\partial^2 v}{\partial x^2}+\frac{\partial^2 v}{\partial y^2}\right) \tag{14}$$

where $Re=U\times L/v$ is the Reynolds number. Similarly, for the particle field, the non-dimensionalized equations for the first three moment equations are given by:

$$\frac{\partial M_0}{\partial t}+u\frac{\partial M_0}{\partial x}+v\frac{\partial M_0}{\partial y}=\frac{1}{ReSc_M}\Delta\left(\frac{(4+5M_C)M_0V^{-2/3}}{9}\right)+Da\frac{(65{M_C}^2-1210M_C-9223){M_0}^2V^{1/6}}{5184}$$
$$\frac{\partial M_1}{\partial t}+u\frac{\partial M_1}{\partial x}+v\frac{\partial M_1}{\partial y}=\frac{1}{ReSc_M}\Delta\left(\frac{(10-M_C)M_0V^{1/3}}{9}\right)$$
$$\frac{\partial M_2}{\partial t}+u\frac{\partial M_2}{\partial x}+v\frac{\partial M_2}{\partial y}=\frac{1}{ReSc_M}\Delta\left(\frac{(7+2M_C)M_0V^{4/3}}{9}\right)-Da\frac{(701{M_C}^2-4210M_C-6859){M_1}^2V^{1/6}}{2592} \tag{15}$$

in which the two dimensional Laplace operator is defined as

$$\Delta=\frac{\partial^2}{\partial x^2}+\frac{\partial^2}{\partial y^2} \tag{16}$$

and the Schmidt number based on the particle moment is given as

$$Sc_M=v/(\kappa/{V_0}^{2/3}) \tag{17}$$

The initial mean particle volume V_0 is determined by the reference moment M_{k0} (i.e., $V_0=M_{10}/M_{00}$) and $M_{c0}=M_{20}\times M_{00}/M_{10}^2$. It should be noted that M_{c0} is the polydispersity index and is unity for monodisperse aerosols (Pratsinis, 1988). The Damkohler number, Da, represents the ratio of the convective time scale to the coagulation time scale and is given by

$$Da=\frac{\sqrt{2}B_1M_{00}{V_0}^{1/6}}{U/L}=\frac{\sqrt{2}B_1M_{10}}{U/L{V_0}^{5/6}} \tag{18}$$

where M_{10} is the initial volume fraction and is defined as the ratio of the volume of the particles to the volume of the fluid–particle mixture. In the temporal mixing layer under consideration, the characteristic length and velocity scales, as well as the volume fraction, are the primary means of controlling the rate of coagulation. These quantities affect directly the

Damkohler number. This non-dimensional number therefore serves as a single parameter to characterize the coagulation growth in the hydrodynamic flow. Damkohler numbers of zero and infinity represent the two limiting flow conditions where zero indicates that the particles do not collide while infinity implies that collisions occur instantaneously, and all particles are instantaneously converted to the largest particle (Settumba & Garrick, 2003; Garrick et al., 2006).

It is obvious that Eq. (15) is the system of partial differential equations and all terms are denoted by the first three moments M_0, M_1 and M_2, and thus the system presents no closure problem. Under these conditions, the first three moments for describing aerosol dynamics are obtained through solving the systems of partial differential equations. Here, the derivation of Eq. (15) for the particle fields does not involve any assumptions for the particle size distribution (PSD), and the final mathematical form is much simpler than the method of moment (MOM) (Garrick et al., 2006; Pratsinis, 1988; Settumba & Garrick, 2003; Yu et al., 2008a, b, c).

2.4. The initial conditions for particles

Initially, the lower stream (stream 2) is free of particles, while the upper stream (stream 1) is populated by nano-particles. The initial particle distribution of the present cases is assumed to be the lognormal distribution; and the size distribution function is defined as (Pratsinis, 1988):

$$n(\upsilon,t)=\frac{N}{3\sqrt{2\pi}\upsilon\ln\sigma}\exp\left(-\frac{\ln^2(\upsilon/\upsilon_g)}{18\ln^2\sigma}\right) \tag{19}$$

in which N is the parameter for the log-normal distribution, and the geometric mean volume and standard deviation are expressed as the functions of the first three moments:

$$\upsilon_g=\frac{{M_1}^2}{{M_0}^{3/2}{M_2}^{1/2}};\ \ln^2\sigma=\frac{1}{9}\ln\left(\frac{M_2M_0}{M_1^2}\right) \tag{20}$$

The initial kth moments M_{k0} are expressed as:

$$M_{k0}=N{\upsilon_g}^k\exp\ (9k^2\ln^2\sigma/2) \tag{21}$$

It should be noted that different researchers use different forms for the width parameter of standard deviation in the lognormal distribution. Under the case of the initial log-normal distribution with $N=1$, $\upsilon_g=3^{1/2}/2$ and $\ln\sigma=(\ln 4/3)^{1/2}/3$ which is consistent with the initial condition used by Barrret & Jheeta (1996), then the initial kth moments for $k=0$, 1, 2 are $M_{00}=1$, $M_{10}=1$ and $M_{20}=4/3$, respectively, in the particle laden stream.

3. Results and discussions

3.1. Numerical methods

The length of the computational domain is chosen as 4π by 4π in the stream-wise and cross-stream directions such that it accommodates exactly two wavelengths of the fundamental perturbation. Throughout the investigation, the value of *Re* is taken as 200, and the Schmidt number based on the particle moment is set to unity for discussion the particle coagulation conveniently in this study. Slip conditions are applied at the upper and lower boundaries of the control volume, that means the zero gradient boundary condition are applied to the y boundaries. The simulations typically employ a discretization mesh consisting of 129 by 129 points in the computational domain. The time advancement is accomplished by means of a fourth-order Runge–Kutta method, and the size of the time step strongly depends on the magnitude of the dimensionless parameters, as they effectively control the range of advection velocities and diffusive or dispersive effects, and each calculation simulated up to a non-dimensional time of $t=45$. The time is long enough for the development of second vortex pairing and rolling up. At the beginning of the simulation, the particle velocities are set equal to the local fluid velocity.

In order to avoid the high costs of performing a simulation, the formation of large-scale structures is expedited through the addition of the disturbances based on the base flow field. The perturbations are introduced in the form of a traveling wave, which is a combination of linear eigenfunctions with fundamental and sub-harmonic disturbances obtained from the linear stability calculations. These perturbations are specified as part of the initial condition superposed on Eq. (2). In other words, the perturbations correspond to the most amplified mode of the two-dimensional Orr–Sommerfeld equation for fundamental and sub-harmonic wave numbers. The stream function of the disturbances flow is given as follows:

$$\psi=\mathrm{Real}\left\{A_1[\phi_1(y)\times e^{i\alpha x}]+A_2[\phi_2(y)\times e^{i\alpha x/2}]\right\} \tag{22}$$

in which A_1 and A_2 are the amplitude of the disturbances, α and $\alpha/2$ represent the dimensionless wave numbers for fundamental and sub-harmonic disturbances, and ϕ_1 and ϕ_2 denote the normalized eigenfunctions for the corresponding perturbations, which can be approximately derived from the in viscid linear instability theory in the case of high Reynolds numbers (Michalke, 1964, 1965). For convenience, the value for α in this study is set to be unit; the criteria for the choice of the perturbation magnitudes were small initially compared to the mean flow, and the fundamental and the sub-harmonic

perturbations initially have amplitude of $A_1=8.12e-3$ and $A_2=2.03e-3$, respectively. These values are very similar to those used in Tong & Wang (1999).

In this paper, the numerical method for modeling fluid flow is based on the MATLAB program mit18086_navierstokes.m (Seibold, 2008), which is used for teaching and learning about incompressible, viscous flows. It is an example of a simple numerical method for solving the Navier–Stokes equations. It contains fundamental components, such as discretization on a staggered grid, an implicit viscosity step, a projection step, as well as the visualization of the solution over time. In the two-dimensional mixing layer and within the parameter ranges studied, the effect of the nano-particle on the formation of the coherent structures such as the ribs and the cups is found to be negligible. The vorticity contours at different time are shown in Fig. 2 to visualize the formation of vortical structure by roll-up and subsequent pairing. Fig. 3 shows the evolution of local vorticity along the centerlines $x=0$ and $y=0$, respectively. The cost of the direct numerical simulation for the vortex evolution of fluid flow from zero to total time $t=40$ with time step $\Delta t=0.01$ is only about 138 s on a personal computer (MacBook Pro with 2.4 GHz CPU). So the numerical method is compact and fast. Based on the MATLAB program, simulations for various Damkohler numbers ($Da=0.5$, 1.0, 2.0) were performed for particle field, which correspond to various initial volume fractions.

3.2. Validations of present particle moment method

In the application of the method of moments, there are two key issues: one issue is to find a suitable method to close the moment equations and another is to reconstruct the particle size distribution using the known moments. In fact,

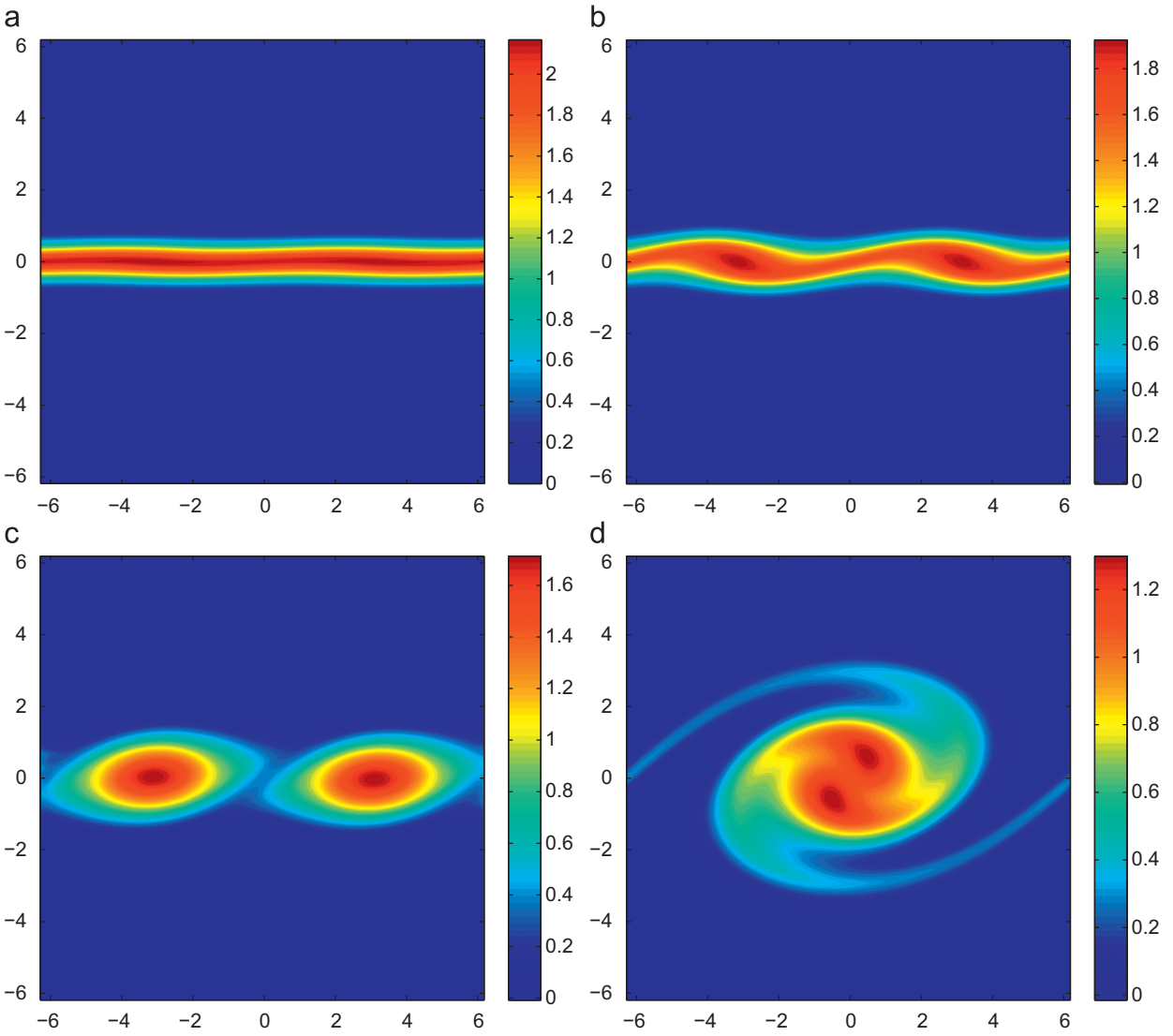

Fig. 2. The evolution of the mixing layer visualized by the vorticity contours, (a) $t=5.5$; (b) $t=11$; (c) $t=22$; (d) $t=44$.

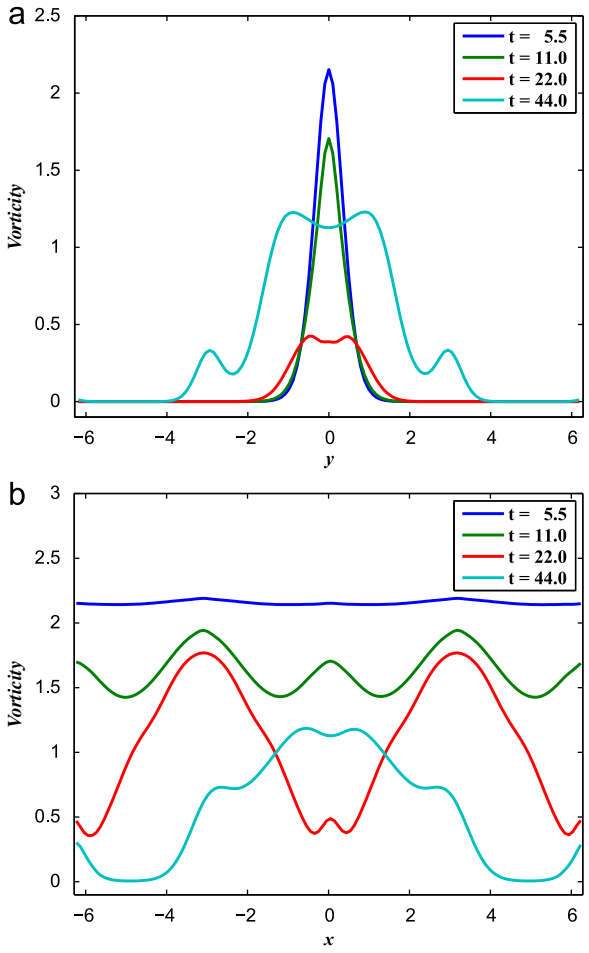

Fig. 3. The evolution of vorticity with time from time $t=5.5$ to 44 along the line cuts at, (a) $x=0$; (b) $y=0$.

since the method of moments was proposed by Hulbert & Katz (1964), many variants have been used, including the first three moment methods proposed by Lee et al. (1984) which is also called by Pratsinis method due to the fact that it was used in his work in 1988, the QMOM proposed by McGraw (1997), the DQMOM (Fox, 2003), and the TEMOM (Yu et al., 2008a). Usually, Lee's method was considered as a method with a prior assumption because in the transformation from particle size space to moment space there is a physical assumption, i.e., the particle size distribution always follow the log-normal distribution with the time. In the QMOM, DQMOM and TEMOM methods, however, there is no requirement for the particle size distribution, and the mathematical form for the fractal and integer moments is completely dependent on the mathematical formulation rather than the physical assumption. For the TEMOM method, the mathematical form of the kth moments is fully dependent on the expanded Taylor-series. Therefore, here we have written, the TEMOM is viewed as a method without any prior assumption on the shape of particle size distribution. In fact, the same observations have been made in McGraw's work for the QMOM method (1997) and Yu's work for TEMOM method (2008). Nowadays, for all the methods of moments, the reconstruction based on the known moments (i.e., the inversion problem) is still not yet well resolved. The reason is that, for some aerosols, they do not usually follow the log-normal distributions. However, if an aerosol follows the log-normal distribution, the reconstruction based on the first three moments can be exactly achieved. The existing studies have shown that it is reasonable to consider that an aerosol follow the log-normal distribution if there is no other internal or external process except coagulation. For the TEMOM method, Yu et al., (2008a, b, c) have provided a validation study of the lognormal distribution for the pure coagulation process using the same collision frequency. In this study, the same coagulation process is involved and thus the validity of TEMOM method is therefore ensured.

In order to validate the TEMOM method in the present study, it is necessary to compare the model with other known methods over long evolution times. Yu et al. (2008a, b, c) have compared the TEMOM model with MOM (Pratsinis, 1988), QMOM (McGraw, 1997) etc., their results showed that the TEMOM model produces the same precision as QMOM with six nodes and MOM models. In addition, the consumed CPU time for the TEMOM is the shortest among all the investigated

models. Therefore, if the present result is consistent with that of Yu et al., then the numerical method is validated. The evolutions of the particle moments and mean particle volume without advection and diffusion are shown in Fig. 4, all the curves overlap with those of Yu et al., and it is difficult to distinguish one from the other. There exists an asymptotic solution for the distribution of reduced particle number in Fig. 4a, and the increased dimensionless particle moment in Fig. 4c. Moments (M_C) along $x=0$ at $t=45$ without disturbance in fluid flow, (a) the distribution of mean particle volume, V; (b) the distribution of dimensionless particle moment, M_C under the conditions $Re=200$, $Sc_M=1$ and $Da=1$, (a) M_0; (b) M_1; (c) M_2; (d) M_c.

An analysis of coagulating aerosols suggests that regardless of the initial size distribution, a self-preserving size distribution is attained in the absence of particle formation or depletion. The so-called self-preserving size distribution has become an important tool to explore the aerosol coagulation mechanisms. The self-preserving form is usually approximated by a lognormal distribution with a geometric standard deviation σ, which can be obtained by solving the dimensionless particle moment in Eq. 20. The asymptotic value of σ for QMOM with six nodes is about 1.346; the asymptotic value of TEMOM is 1.345 (Yu et al., 2008a, b,c); in addition, the asymptotic value for MOM is 1.355 (Pratsinis, 1988), which is close to the value given by Lee et al. (1984) who used log-normal functions for particle size distribution. Fig. 4c shows the variations of dimensionless particle moment M_C with time in the free molecular regime. We can see that the self-preserving size distribution attains for all methods at about $t=5$, and the asymptotic value of M_C is 1.6494, which is different from the value 2.1633 give by Yu et al. (2008a, b, c) calculated with Eq. 20. The reason is that the value of moments in the present study has been non-dimensionalized, if the particle second moments multiplied with its initial value $M_{20}=4/3$, then both results will be consistent with each other.

The effect of grid resolution on the accuracy of particle moments is shown in Fig. 5. For a convenient comparison, the disturbance flow is set to zero, the other parameters remains unchanged. The figure shows that the mean particle volumes remain consistent with one another at various grids; but the dimensionless particle moment is somewhat sensitive to the

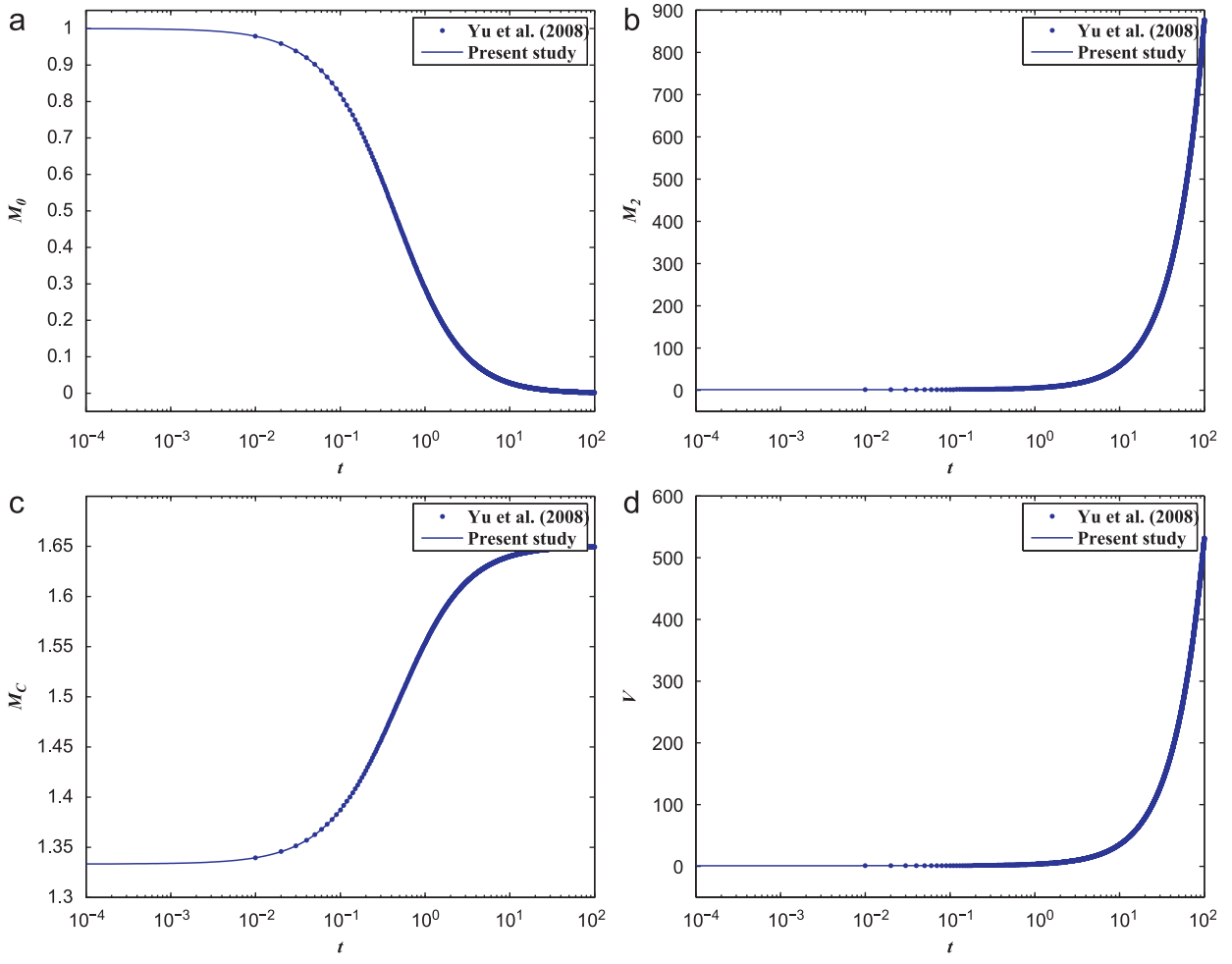

Fig. 4. Comparison for time evolution of particle moments without diffusion and convection.

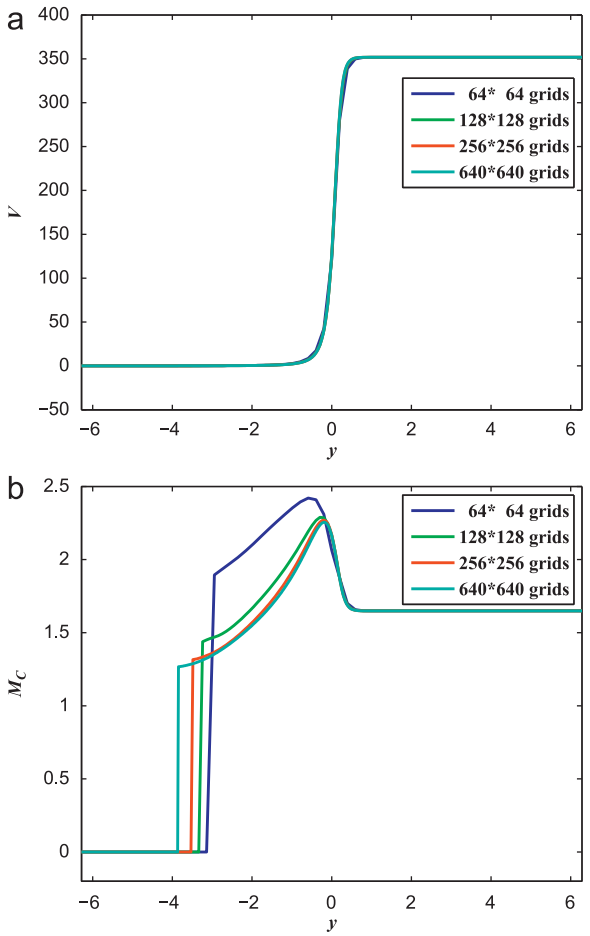

Fig. 5. The effect of resolution on the accuracy of mean particle volume (V) and dimensionless particle moment (MC).

grid resolution. Generally, the higher the resolution, the more accurate of the numerical results are, but for the higher resolution, the computation cost also increases dramatically. Because the diffusion coefficient is the function of time and position, to obtain the correct result, the time step will also need to be refined than that determined by the normal CFL conditions to avoid numerical diffusion or dispersion, and the computing cost will increase rapidly, so the resolution at 129×129 represents a good balance between accuracy and computing cost. At the same time, the value of M_C in the neighborhood of the interface between the particle laden and particle free domain is greater than that in other places, which is brought out by the combination of coagulation and diffusion, it reveals that the change rate for coagulation is much larger than that due to diffusion under the given conditions. The reason is that the maximum value of M_0 occurs in the neighborhood of the interface due to the greater changing rate for coagulation, the particles will be transported from higher to lower particle number concentration zones due to diffusion. The similar distribution occurs for the other particle moments, M_1 and M_2. If the particles near the interface were transported to the particles laden zones, the particle volume concentration in some places will increase and exceeds unit slightly, but the change rate for mass distribution is small due to the smaller diffusion mechanism, then the peak of M_C occurs near the interfaces.

3.3. Evolution of vortical structure and particle moments

Outside the large-scale eddies in the flow domain, the behavior of the coagulation is similar to that for the zero-dimensional case, i.e., the 0th order moment decreases exponentially with time, and the first order moment remains invariant, and the second order moment increases with time approximate linearly. The effect of advection and diffusion or the flow coherent structure on the particle coagulation is small. However, the role of the advection in the large-scale vortex motion area is significant, and the distribution of the first three moments reflects the distortion and mixing induced by the vortex structure in the mixing layer as shown in Fig. 7. The effect of the advection on the evolution of particle coagulation can also be found in Fig. 6.

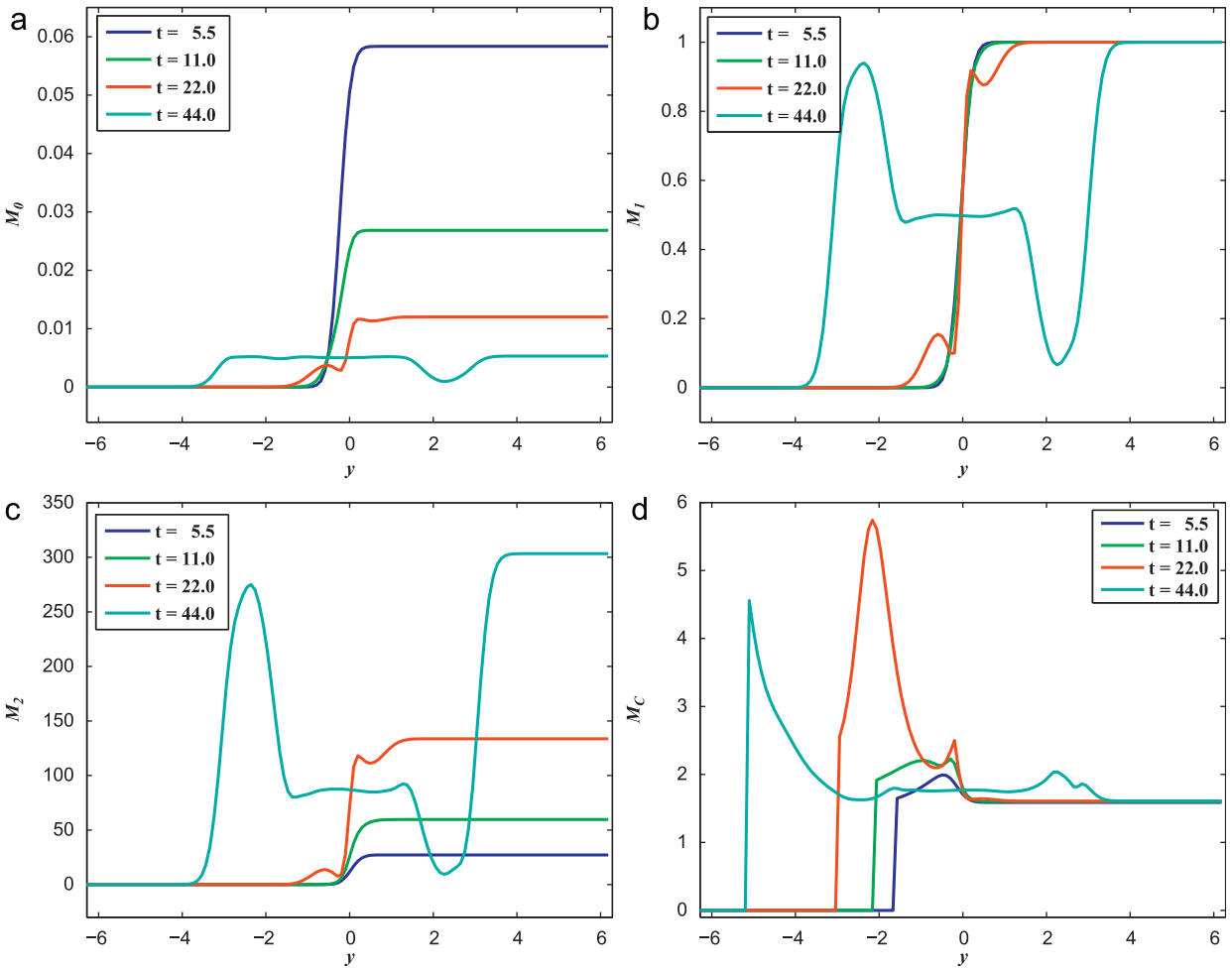

Fig. 6. The evolution of the particle moments with time at t=5.5, 11, 22, 44 along the line x=0.

Evolution of the 0th moment M_0 in the cross-stream direction at x=0 is shown in Fig. 6a, in which the Damkohler number is unity. The result shows that the total particle number concentration, which is represented by M_0 decreases as the particles collide and coagulate. Fig. 6a also reveals the M_0 is reduced exponentially as the time is advanced, which corresponds to the nonlinear growth rate due to coagulation. At t=44, the value of M_0 in the upper stream of the flow domain has decreased from 1.0 to 0.0058. At the same time, the value of M_0 in certain region near the neighborhood of the interface between the particle-laden and particle-free streams is smaller than that of other place in the upper fluid, which is brought out by the combination of coagulation, diffusion and advection. It should be noted that near the lower boundary of the flow domain, the particle number concentration increases with time. This represents the advection and diffusion of particles towards to the lower stream that is free of particles initially.

The evolution of M_1 under the same conditions is shown in Fig. 6b. The particle mass outside of fluid vortex remains unchanged in the time period from t=5.5 to 44. The value of M_1 develops an anti-symmetric profile relative to the mean value, in the cross-stream direction inside of the fluid vortex. Mass increase of particles in the lower stream zones is equal to the mass decrease in the upper stream regime at the same distance to the core of vortex, and the total particle mass over the entire flow field is conserved.

In an initially mono-disperse aerosol, the coagulation creates new particles of different sizes and increases the size of each particle. These processes are indicated by the evolution of the second particle moment, which is shown in Fig. 6c. Generally, the second moment increases throughout the flow field contained with particles, except that some decreasing area caused by advection and diffusion in the upper stream. However, the changes along the cross-stream are different, which is similar with the changes of the 0th particle moment, but the rate of changes is different, i.e., in general the number concentration is decreasing exponentially, while the second moment of particles is increasing approximate linearly with time without advection and diffusion.

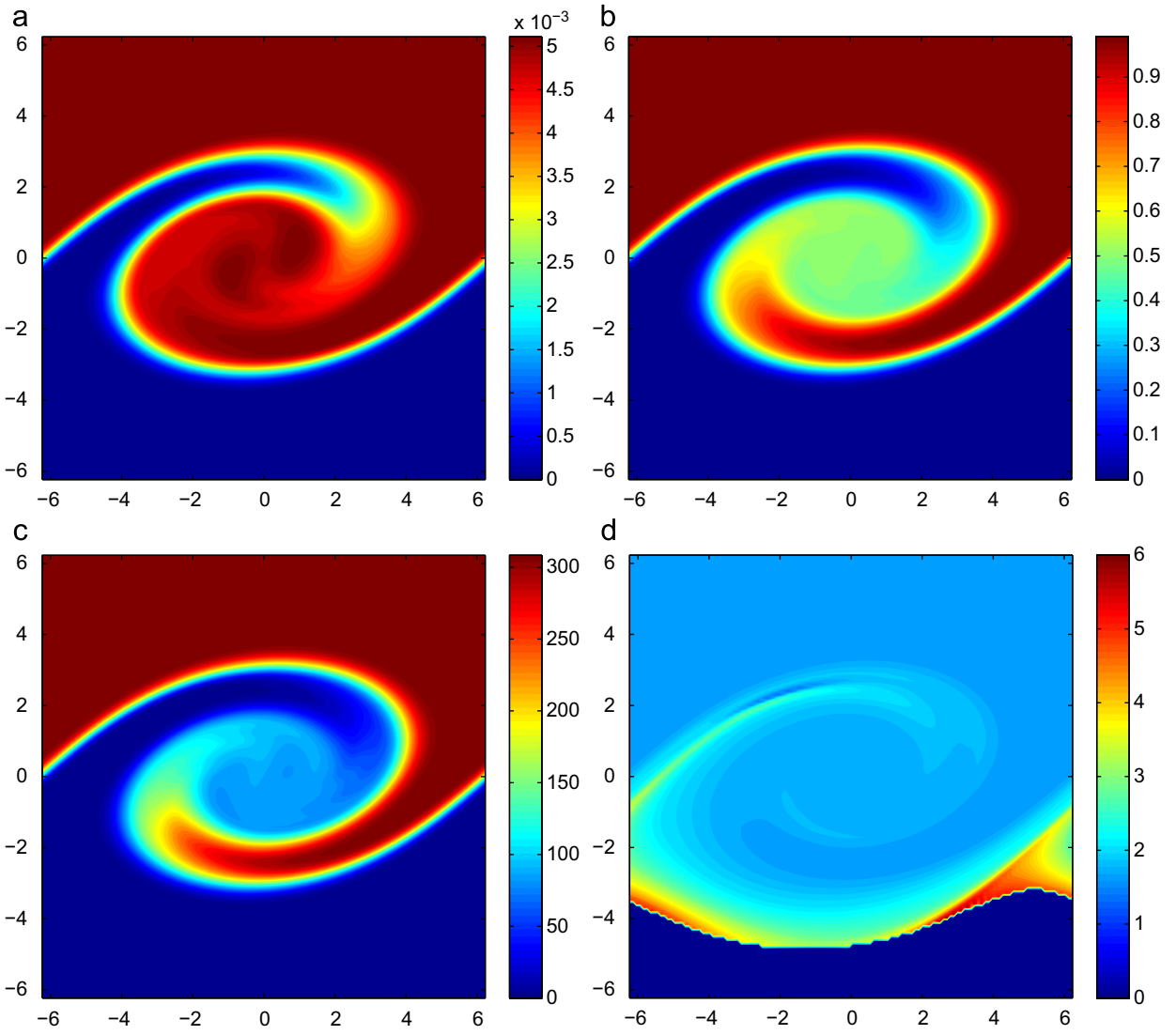

Fig. 7. The contour of the particle moments at time $t=45$ under the conditions $Re=200$, $Sc_M=1$ and $Da=1$, (a) M_0; (b) M_1; (c) M_2; (d) M_c.

The evolution and distribution of dimensionless particle moment are shown in Figs. 6 and 7d. The figures demonstrate that the dimensionless particle moment under the advection of vortex retains the similar characteristic with the results without disturbances as shown in Fig. 5b, i.e., the maximum value of M_0 occurs in the neighborhood of the interface. Because that the standard deviation is highly sensitive to resolution, the present results contain some effect of numerical diffusion; nevertheless the distribution shape is consistent with that of Settumba & Garrick (2003) at 1500×1500 resolution.

The particle volume increases at all locations in the flow field, which is shown in Fig. 8. The mean particle volume is also sensitive to resolution, but its evolution and distribution is more accurately simulated than that of dimensionless particle moment. Comparison with the evolution contours between mean particle volume and vortex, it can be found that the two structures are similar with each other at different time from $t=5.5$ to 44. The results also show that the particle volume increases rapidly as time advances.

From the distribution of the first three particle moments in Fig. 6, it can be seen that the characteristic of distribution curves for different moments are closely related to that of vortex structure in the mixing layer, which is shown in Fig. 3a. In the upper stream, the concentration of particles is reduced due to the introduction of particle-free fresh fluid by the vortex, and the three moments are decreased in the corresponding area; while in the lower stream, the situations is just the opposite. In the core of the vortex, the distribution of three moments for a long time at $t=44$ is smooth and uniform relatively due to the combination of coagulation, advection and diffusion.

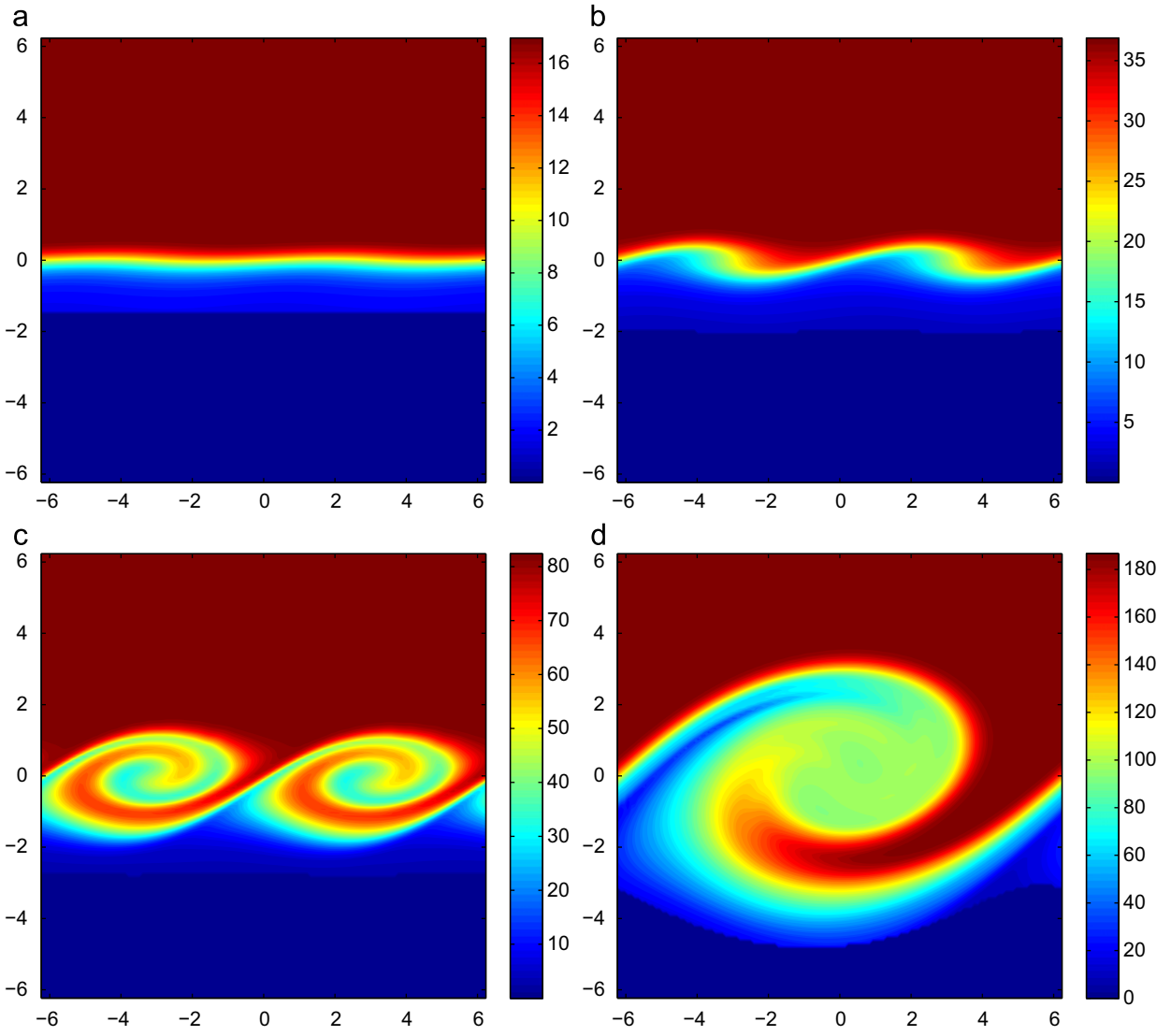

Fig. 8. The evolution and distribution of mean particle volume ($V=M_1/M_0$) with time under the conditions $Re=200$, $Sc_M=1$ and $Da=1$, (a) $t=5.5$; (b) $t=11$; (c) $t=22$; (d) $t=44$.

3.4. *Effect of Damkohler number*

The particle coagulation Damkohler number, *Da*, represents the ratio of advection to coagulation time scales in the moments equations (Settumba & Garrick, 2003). The larger the Damkohler number; the smaller the characteristic coagulation time scale; or the greater generation rate of large size particles. The effects of Damkohler number ($Da=0.5$, 1, 2) on the mean particle volume due to coagulations are shown in Fig. 9. Together with Fig. 8d, the figures show that the distribution of mean particle volume at different Damkohler numbers is similar to the structure of the vortex as shown in Fig. 2d. The evolutions of the particle 0th (and second) moments exhibit three distinct levels, representing the effect of characteristic coagulation time scale as shown in Fig. 10 in the cross-stream direction at $x=0$. The figures in Fig. 10 also reveal that the values of moments change greatly as the Damkohler number increases. The increase in the Damkohler number reduces the relative contribution of diffusion and advection, which consequently affects the spatial distribution of particle moments, and produces a smoother distribution for 0th particle moment or steeper distribution for second particle moment and mean particle volume distribution in space. The mean particle volume increases at all locations in the flow field, the larger the Damkohler number, and the greater generation rate of large-size particles. The distribution of particle average diameter can also be determined by the relation [$d_{\mathrm{pavg}}=(6V/\pi)^{1/3}$]. The normalized distribution corresponding to Fig. 10 is shown in Fig. 11. The results show that all the distributions are self-similarity. The asymptotic analysis reveals that the relative growth rate is slow at

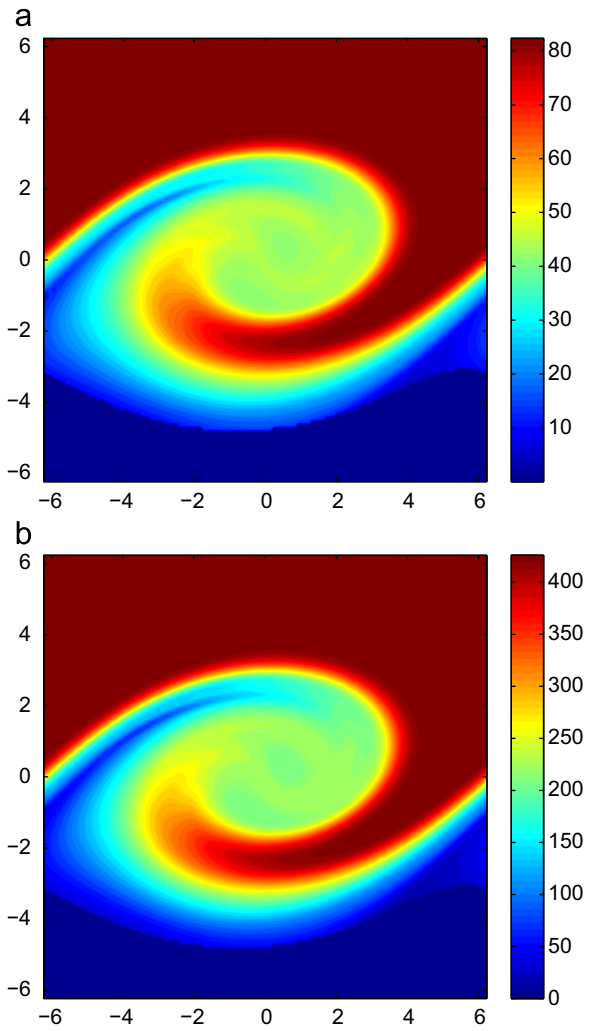

Fig. 9. The distribution of mean particle volume at $t=44$ under the fluid flow conditions $Re=200$, $Sc_M=1$, (a) $Da=0.5$; (b) $Da=2$.

long times, and the local Damkohler number becomes smaller, showing the coagulation is slow, and the system bottleneck is the advection and diffusion, this explains why the distributions are self-similar. This self-similarity implies that the effect of coagulation and effect of mixing by advection and diffusion on particle growth could be modeled separately.

In summary, the particle coagulation affects quantitatively the distribution of particle volume concentration and average diameter, but the qualitative characteristics of these distributions remain unchanged. The Damkohler number has little effect on the distribution of local mass, and the distribution profiles of particle first order moments is effected and dominated by the advection due to vortex evolution in the temporal mixing layer.

4. Conclusions

In this study, numerical simulation of nanoparticle coagulation in the temporal mixing layer was performed without the presence of a temperature gradient. The flow field was obtained by solving the incompressible Navier–Stokes equations coupled with the Orr–Sommerfeld equation. The formation of large-scale structures is expedited through the addition of fundamental and sub-harmonic perturbations based on the linear stability theory. Taylor series expansion method of moments (TEMOM) was used to approximate the coagulation of particle in the general dynamic equations (GDE). The flow and particle fields are coupled together, and there are three non-dimensional parameters in the governing equations (i.e., Reynolds number, Re; Schmidt number based on particle moment, Sc_M, and Damkohler number, Da).

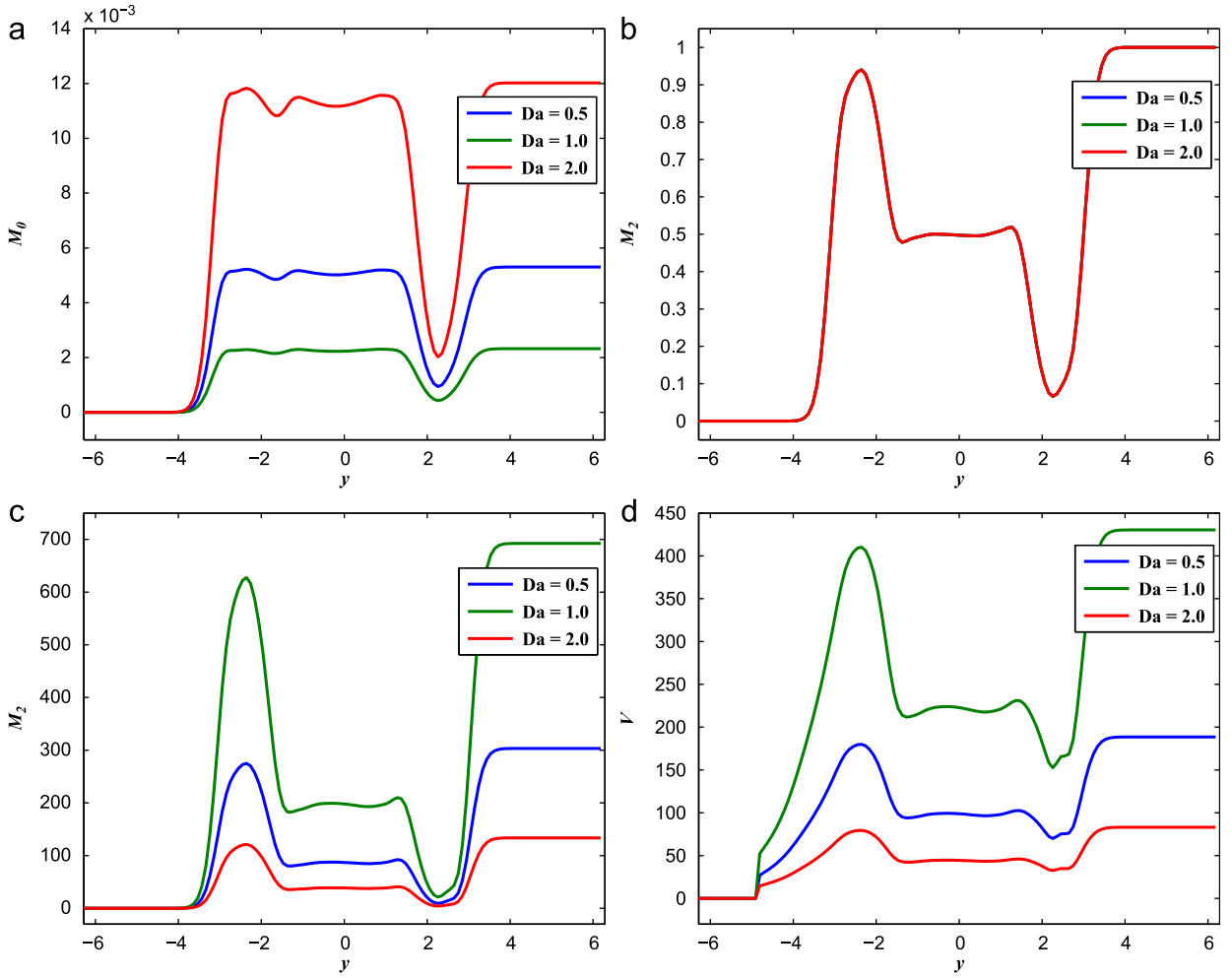

Fig. 10. The distribution of particle moments and mean particle volume for different Damkohler numbers at $t=44$, (a) M_0; (b) M_1; (c) M_2; (d) V.

Direct numerical simulation for three different Damkohler numbers ($Da=0.5, 1, 2$) were performed under a given the flow condition ($Re=200$) and particle moment Schmidt number ($Sc_M=1$). Generally, the total particle number concentration decreases, and total particle mass in the fluid remains unchanged, and the second particle moment increases as the particles collide and coagulate far away from the interface in the particle-laden stream. The effect of the fluid advection on particle coagulation is small outside of the eddy structure; however, the particle coagulation within the eddy core resembles the vortices' structure because of the large-scale eddy motion. The results reveal that the coherent structure plays a significant role on the particle coagulation in a temporal mixing layer. The Damköhler number dominates the structure of the particle volume in the neighborhood of the interface and the core of vortex. For a low Damköhler number flow, the distribution of particle number concentration near the interface is non-uniform and exhibits the characteristics of vorticity distribution inside the vortex structure. As the Damköhler number increases, the gradient decreases; while the situation is opposite for the second particle moment. The particle volume increases at all locations in the flow field, the larger the Damkohler number, and the greater generation rate of large-size particles. Nevertheless, we observe a self-similar behavior when the moments are normalized by their respective value in the well-mixed region outside the vortical structure. This indicates that the effect of coagulation and effect of mixing by advection and diffusion on particle growth can be modeled separately.

This study represents a first effort to demonstrate how the efficient TEMOM method can be integrated into a flow solver to model particle growth in an inhomogeneous flow system. The TEMOM method is as accurate as other state-of-the-art moment-based methods but is computationally more efficient. There are several possible extensions of the study. We only considered a specific collision frequency and other modified and more realistic collision frequency formulation should be introduced as the particles grow in size. Other growth mechanisms including particle inertia must also be considered. Thermal effects related to the flow and particle phase transformation in a reactive system could be incorporated as well. Experimental observations of particle distributions in inhomogeneous flow systems would be very helpful in validating our approach.

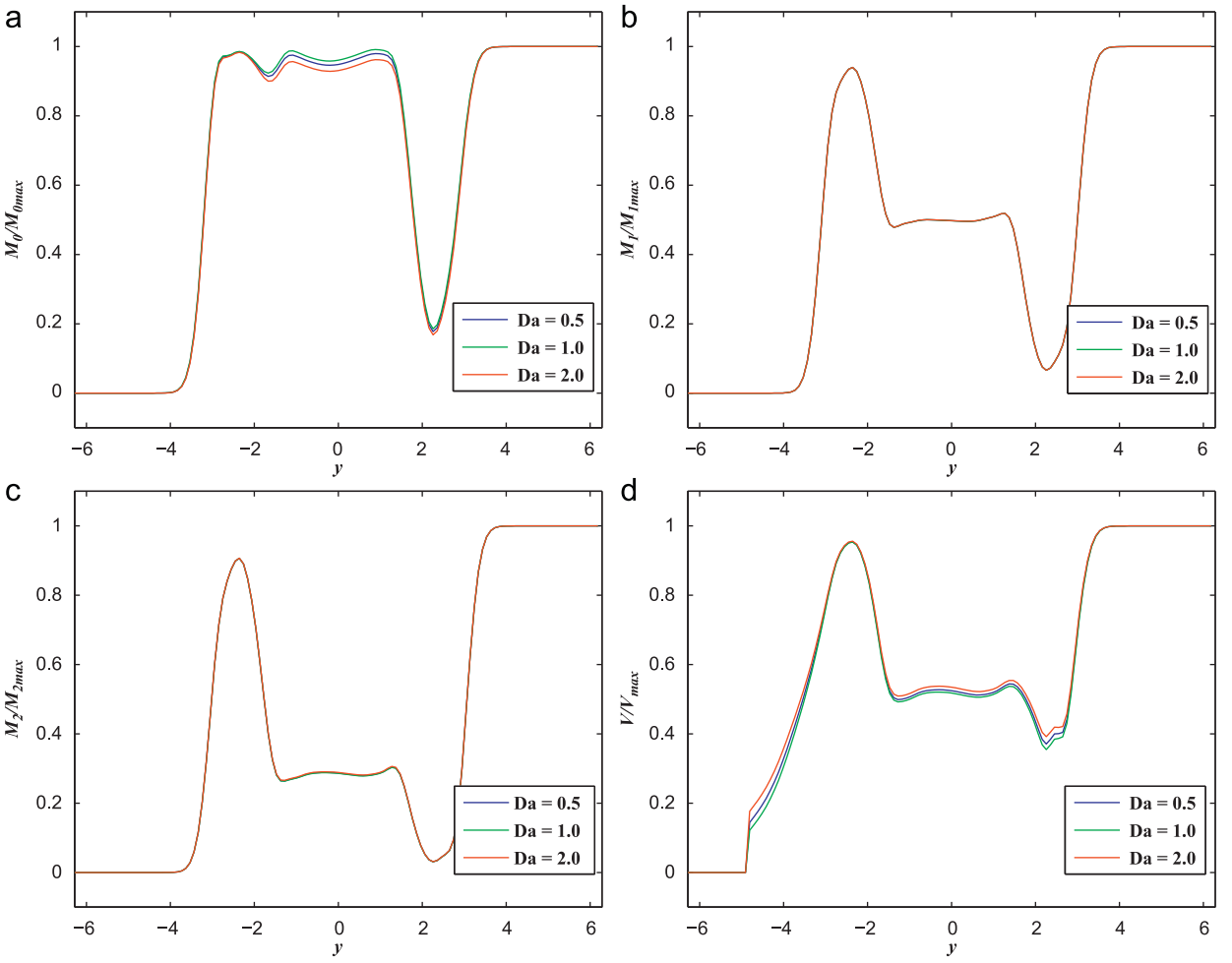

Fig. 11. The normalized distribution of particle moments and mean particle volume for different Damkohler numbers at $t=44$, (a) M_0; (b) M_1; (c) M_2; (d) V.

Acknowledgements

This work is supported by the National Natural Science Foundation of China with Grant no. 50806023, and the National Natural Science Foundation of China with Grant No. 50721005, and the Programmer of Introducing Talents of Discipline to Universities ("111" project No. B06019) China; and US National Science Foundation through OCI-0904534.

References

Barrret, J.C., & Jheeta, S.J. (1996). Improving the accuracy of the moments method for solving the aerosol general dynamic equation. *Journal of Aerosol Science*, *27*, 1135–1142.
Chan, T.L., Lin, J.Z., Zhou, K., & Chan, C.K. (2006). Simultaneous numerical simulation of nano and fine particle coagulation and dispersion in a round jet. *Journal of Aerosol Science*, *37*, 1545–1561.
Davidson, C.I., Phalen, R.F., & Solomon, P.A. (2005). Airborne particulate matter and human health: a review. *Aerosol Science and Technology*, *39*, 737–749.
Fox, R.O. (2003). *Computational Models for Turbulent Reacting Flows*. Cambridge University Press: Cambridge.
Friedlander, S.K. (2000). *Smoke, Dust, and Haze: Fundamentals of Aerosol Dynamics* 2nd ed.). Oxford University Press: London.
Garrick, S.C., Lehtinen, K.E.J., & Zachariah, M.R. (2006). Nanoparticle coagulation via a Navier Stokes nodal methodology: evolution of the particle field. *Journal of Aerosol Science*, *37*, 555–576.
Hulbert, H.M., & Katz, S. (1964). Some problems in particle technology: a statistical mechanical formulation. *Chemical Engineering Sciences*, *19*, 555–574.
Jacobson, M.Z., Kittelson, D.B., & WattsW., F. (2005). Enhanced coagulation due to evaporation and its effect on nanoparticle evolution. *Environmental Science & Technology*, *39*, 9486–9492.
Kittelson, D.B. (1998). Engines and nanoparticles: a review. *Journal of Aerosol Science*, *29*, 575–588.
Lee, K.W., Chen, H., & Gieseke, J.A. (1984). Log-normally preserving size distribution for Brownian coagulation in the free-molecule regime. *Aerosol Science and Technology*, *3*, 53–62.
Lin, J.Z., & Liu, Y.H. (2010). Nanoparticle nucleation and coagulation in a mixing layer. *Acta Mechanica Sinic*, *26*, 521–529.
Lin, J.Z., Shi, X., & Yu, Z.S. (2003). The motion of fibers in an evolving mixing layer. *International Journal of Multiphase Flow*, *29*, 1355–1372.
McGraw, R. (1997). Description of aerosol dynamics by the quadrature method of moments. *Aerosol Science and Technology*, *27*, 255–265.
Michalke, A. (1965). On the growing disturbances in an inviscid shear layer. *Journal of Fluid Mechanics*, *23*, 521–544.

Michalke, A. (1964). On the inviscid instability of the hyperbolic tangent velocity profile. *Journal of Fluid Mechanics*, *19*, 543–546.
Miller, S.E., & Garrick, S.C. (2004). Nanoparticle coagulation in a planar jet. *Aerosol Science and Technology*, *38*, 79–89.
Moser, R.D., & Rogers, M.M. (1993). The three dimensional evolution of a plane mixing layer: pairing and transition to turbulent. *Journal of Fluid Mechanics*, *247*, 275–320.
Prakash, A., Bapat, A.P., & Zachariah, M.R. (2003). A simple numerical algorithm and software for solution of nucleation, surface growth, and coagulation problems. *Aerosol Science and Technology*, *37*, 892–898.
Pratsinis, S.E. (1988). Simultaneous nucleation, condensation, and coagulation in aerosol reactor. *Journal of Colloid and Interface Science*, *124*, 416–427.
Pratsinis, S.E., & Kim, K.S. (1989). Particle coagulation, diffusion and thermophoresis in laminar tube flows. *Journal of Aerosol Science*, *20*, 101–111.
Rogers, M.M., & Moser, R.D. (1992). The three dimensional evolution of a plane mixing layer: the Kelvin–Helmholtz rollup. *Journal of Fluid Mechanics*, *243*, 183–226.
Seibold B. (2008): A compact and fast Matlab code solving the incompressible Navier Stokes equations on rectangular domains. ⟨http://www-math.mit.edu/∼seibold/⟩.
Settumba, N., & Garrick, S.C. (2003). Direct numerical simulation of nanoparticle coagulation in a temporal mixing layer via a moment method. *Journal of Aerosol Science*, *34*, 149–167.
Stone, V., & Donaldson, K. (1998). Small particles-big problem. *The Aerosol Society Newsletter*, *33*, 12–14.
Tong, X.L., & Wang, L.P. (1999). Two-way coupled particle laden mixing layer. Part 1: Linear instability. *International Journal of Multiphase Flow*, *25*, 575–598.
Upadhyay, R.R., & Ezekoye, O.A. (2003). Evaluation of the 1-point quadrature approximation in QMOM for combined aerosol growth laws. *Journal of Aerosol Science*, *34*, 1665–1683.
Wang, L.P., Xue, Y., & Grabowski, W.W. (2007). A bin integral method for solving the kinetic collection equation. *Journal of Computational Physics*, *226*, 59–88.
Xie, M.L., Lin, J.Z., & Xing, F.T. (2007). On the hydrodynamic stability of a particle laden flow in growing flat plate boundary layer. *Journal of Zhejiang University-Science A*, *8*, 275–284.
Xie, M.L., Lin, J.Z., & Zhou, H.C. (2009a). Temporal stability of a particle-laden Blasius boundary layer. *Modern Physics Letter B*, *23*, 203–216.
Xie, M.L., Lin, J.Z., & Zhou, H.C. (2009b). The effect of non-linear interaction between gas and particle velocities on the hydrodynamic stability in the Blasius boundary layer. *International Journal of Non-linear Mechanics*, *44*, 106–114.
Yu, M.Z., Lin, J.Z., & Chan, T.L. (2008a). A new moment method for solving the coagulation equation for particles in Brownian motion. *Aerosol Science and Technology*, *42*, 705–713.
Yu, M.Z., Lin, J.Z., & Chan, T.L. (2008b). Numerical simulation of nanoparticle synthesis in diffusion flame reactor. *Powder Technology*, *181*, 9–20.
Yu, M.Z., Lin, J.Z., & Chan, T.L. (2008c). Effect of precursor loading on non-spherical TiO_2 nanoparticle synthesis in a diffusion flame reactor. *Chemical Engineering Science*, *63*, 2317–2329.